Journal of Anatomy

J. Anat. (2008) **212**, pp736–746 doi: 10.1111/j.1469-7580.2008.00899.x

Cranial performance in the Komodo dragon (*Varanus komodoensis*) as revealed by high-resolution 3-D finite element analysis

Karen Moreno,[1] Stephen Wroe,[1] Philip Clausen,[2] Colin McHenry,[1,2,3] Domenic C. D'Amore,[4] Emily J. Rayfield[5] and Eleanor Cunningham[6]

[1]*School of Biological, Earth and Environmental Sciences, University of New South Wales, Australia*
[2]*School of Engineering, University of Newcastle, New South Wales, Australia*
[3]*School of Environmental and Life Sciences, University of Newcastle, New South Wales, Australia*
[4]*Graduate Program in Ecology & Evolution, Rutgers University, New Brunswick, NJ, USA*
[5]*Department of Earth Sciences, University of Bristol, UK*
[6]*Newcastle Mater Misericordiae Hospital, Waratah, New South Wales, Australia*

Abstract

The Komodo dragon (*Varanus komodoensis*) displays a unique hold and pull-feeding technique. Its delicate 'space-frame' skull morphology differs greatly from that apparent in most living large prey specialists and is suggestive of a high degree of optimization, wherein use of materials is minimized. Here, using high-resolution finite element modelling based on dissection and *in vivo* bite and pull data, we present results detailing the mechanical performance of the giant lizard's skull. Unlike most modern predators, *V. komodoensis* applies minimal input from the jaw muscles when butchering prey. Instead it uses series of actions controlled by postcranial muscles. A particularly interesting feature of the performance of the skull is that it reveals considerably lower overall stress when these additional extrinsic forces are added to those of the jaw adductors. This remarkable reduction in stress in response to additional force is facilitated by both internal and external bone anatomy. Functional correlations obtained from these analyses also provide a solid basis for the interpretation of feeding ecology in extinct species, including dinosaurs and sabre-tooth cats, with which *V. komodoensis* shares various cranial and dental characteristics.
Key words behaviour; feeding ecology; finite element; *Varanus komodoensis*.

Introduction

The unusual biology and ecology of the Komodo dragon (*Varanus komodoensis*) have been the focus of much scientific and popular interest. This Indonesian varanid is the largest living lizard, the largest animal known to reproduce by parthenogenesis, and one of only two varanids that commonly feed on prey larger than themselves (Auffenberg, 1981; Watts et al. 2006). This last fact is especially interesting because its feeding performance depends on a combination of behavioural and anatomical features that are not present in other extant terrestrial vertebrates, but might be comparable to those evident in some extinct reptiles, including theropod dinosaurs.

Varanus komodoensis has a broad dorsoventrally compressed skull and its mandible is curved so that the distal-most teeth of the dentary are more medially placed than the mesial teeth. Consequently, there is a wide gap between the upper and lower tooth row in the distal jaw during occlusion (Auffenberg, 1981). Tooth orientation and shape varies along the jaw. Maxillary teeth are more distally curved and laterally oriented than those of the dentary and premaxilla. These characteristics contrast with the morphology of most other varanids, which have relatively narrow rostra, straight mandibles with typically vertical teeth, and comparatively higher skulls (Auffenberg, 1981). In addition, the teeth of *V. komodoensis* are more laterally compressed than those of any other lizard (Mertens, 1942).

Analysis of its feeding behaviour shows that when feeding the Komodo dragon secures the flesh of the prey item between the distal teeth of one side of the muzzle, while cutting with the opposing side. The distal-most crowns are the most bladelike and enter the prey first, followed sequentially by subsequent mesial teeth, each penetrating deeper than the previous tooth. The muzzle is also simultaneously moved laterally in an arc. This motion may be repeated several times on either side until the section is thoroughly separated. Posterior motion of the neck and forelimbs typically assist these feeding movements. Together

Correspondence
Dr K. Moreno, School of Biological, Earth and Environmental Sciences, University of New South Wales, NSW 2052, Australia.
E: dinohuella@yahoo.com

Accepted for publication *12 March 2008*

Table 1 Bill of materials for heterogeneous finite element model of *Varanus komodoensis* skull. The homogeneous model differs only in that it comprises solely 'brick' elements of material property 3

Material	Mass (g)	Volume (mm^3)	Volume (%)	Elastic modulus (E) (MPa)	Density ($g\ mm^{-3}$)
1	13	5 901	15	1 869	0.00029
2	19	8 755	22	10 787	0.00011
3	23	10 381	27	27 082	0.00219
4	31	14 091	36	38 575	0.00286
Total	*86*	*39 129*	*100*		
Beams and trusses in half model					
ID	Type	Length (mm)	Amount of beams	Mass (g)	Estimated force (N)
1	Jaw hinge	10	1	0.02	–
2	MAEMa	30	2	0.60	6
3–7	MAEMb	29	21	1.46	15
8	MAEMc	28	2	0.63	7
9	MAEMd	20	7	0.73	11
10	MPST-S	14	7	0.82	18
11	MPST-P	29	2	0.25	3
12	MAMP	11	5	0.34	9
13	MPT	29	7	2.00	21
14	Interdental beam	–	1	0.05	–

MAEM (a–d) = *m. adductor externus mandibulae*; MPST-S = *m. pseudotemporalis superficialis*; MPST-P = *m. pseudotemporalis profundus*; MAMP = *m. adductor mandibulae posterior*; MPT = *m. pterygoid*.

these actions facilitate the removal of large portions of meat with minimal tearing or shearing (Auffenberg, 1981). Dismembering the prey item usually occurs through defleshing at joints and the application of quick jerks to separate carcass portions. No evidence has been found for bone crushing behaviour in either disarticulation or accessing of bone nutrients (Auffenberg, 1981) and *V. komodoensis* appears to be a flesh specialist that typically avoids extensive tooth–bone contact during defleshing (D.D. personal observation). Swallowing is the result of inertial feeding. During this process, the intramandibular hinge is flexed, allowing expansion of the lower jaw to accommodate large chunks of meat. Carcass portions with skeletal material are readily swallowed whole. This food reduction technique contrasts with that of other varanids, which generally process prey through the application of puncture crushing, followed by side-to-side, tongue-based and inertial transports (Elias et al. 2000; Reilly et al. 2001; Mayes et al. 2005).

In the present study we apply finite element (FE) analysis of three-dimensional (3D) computer models to determine whether mechanical adaptations in the Komodo dragon's skull reflect or facilitate these unique anatomical and feeding characteristics. One of the major advantages offered by the FE approach over more traditional methods is its ability to account for the influence of variable bone properties on mechanical behaviour (Thomason, 1995). The FE models presented here include the first to accommodate multiple bone properties for any reptile. A further aim has been to investigate differences between single property (homogeneous) and more realistic heterogeneous (multiproperty) FE models, to provide insight into the influence of this factor.

Materials and methods

Data collection

The *V. komodoensis* skull used in the present study is from a young adult male (AM R106933) with a snout-tail length of 1.6 m. Maximal length, height and width of the cranium are 142 mm, 34 mm, and 68 mm, respectively. Protocols for model assembly largely follow those described elsewhere (McHenry et al. 2007; Wroe et al. 2007a,b). A 3D FE computer simulation of the skull was generated on the basis of computerized tomography X-ray (CT) scan data (see details below). Masticatory muscles were dissected following protocols developed by Herrel et al. (1999b, 1998) so as to obtain specimen specific fibre lengths and masses with which to estimate cross-sectional areas and calculate muscle forces (Table 1). Due to high variability of muscle fibre orientation, the pennation angles were not taken into account by Herrel et al. (1999b, 1998). These data were used as inputs for the FE model.

CT scanning was conducted at the Mater Hospital, Newcastle, NSW, using a Toshiba Aquilon 16 scanner CT. Slices were 1 mm thick with an inter-slice distance of 0.8 mm, and a field of view (FoV) of 240 mm diameter (200 slices in total). Surface meshes were generated from the CT data and then converted to solid meshes in STRAND7 finite element analysis software. The cranium and mandible were meshed separately and converted into a high-resolution 1.2 million 'brick' element model, with each element modelled as low order (four-noded) tetrahedral 'brick'. Each brick was then assigned a group (one of four, A to D) on the basis of four mean X-ray attenuation values (Hounsfield units, HU) obtained in the different locations within the skull bone. These mean HU were converted into density and its equivalent elasticity modulus

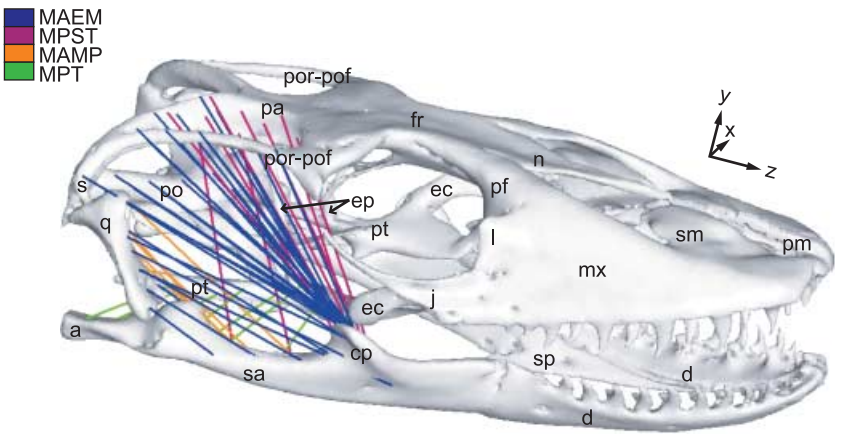

Fig. 1 FE model showing distribution of pretensioned muscle trusses (Table 1). MAEM: *m. adductor externus mandibulae*; MPST = *m. pseudotemporalis superficialis and profundus*; MAMP = *m. adductor mandibulae posterior*; MPT = *m. pterygoid*; a, articular; cp, coronoid process; d, dentary; ec, ectopterygoid; ep, epipterygoid; fr, frontal; j, jugal; l, lacrimal; mx, maxilla; n, nasal; pa, parietal; pf, prefrontal; pm, premaxilla; po, prootic; por-pof, postorbital + postfrontal; pt, pterygoid; qu, quadrate; sa, surangular; sm, septomaxilla; s, squamosal; sp, splenial.

by using an adaptation of the formulas generated by Rho et al. (1995) and Schneider et al. (1996). The resulting distribution of differing bone densities through the skull is such that material group A (lowest density) is mainly placed in symphysis and joint surfaces, material B is generally surrounding material A, and material C is distributed about material D (highest density), which is mainly located on tooth and bone edges. For the heterogeneous model the groups A, B, C and D correspond to materials 1, 2, 3 and 4, respectively (Table 1), and in homogeneous models all the bricks (groups A to D) were conferred material property 3.

Finite element modelling

The skull model was aligned with the general coordinate system, halved and mirrored, to facilitate the rest of the modelling process. The cranium and mandible remain as single objects, in which the articular-quadrate joint is the only movable joint. To model the articular-quadrate joint, we used a hinged beam linked to both upper and lower jaws. Other joints and sutures might acquire some degree of flexibility due to the presence of low HU in the CT, and hence automatically converted to a more elastic material property.

Masticatory muscle origin and insertion areas were identified on the solid model surface based on both dissection of the specimen and details published in Haas (1973). Muscles were modelled as pre-tensioned trusses (members that can only carry axial loads) connecting each insertion area, hence following the main directions of the forces. We calculated truss number as proportional to muscle force (Table 1) and distributed them evenly on the surface of the respective origin/insertion areas following mean muscle action lines (Fig. 1). These techniques produce two advantages: (1) the 3D geometry and lines of action are more accurately captured and (2) forces are more evenly and accurately distributed than in models which reduce primary muscle groups to single vectors.

Bite loading cases were modelled using beams (2 mm diameter, E = 3GPa, 0.3 Poisson's Ratio) located between upper and lower teeth (interdental beam). In bilateral loading cases these beams were reinforced with a rigid link connecting their midpoint.

To prevent free body rotation, FE models must be fixed in space. Point constraints (restricted to single or small numbers of nodes) can produce pronounced artefacts and inaccurate results (Dumont et al. 2005). We applied more realistic constraints using rigid link frameworks at the occipital condyle and tooth bite points to distribute forces.

Loading cases

Adductor muscles were simultaneous and forces bilateral for all load cases, in agreement with results from previous experiments performed on *Varanus exanthematicus*, teiid lizards and crocodilians (Smith, 1982; Busbey, 1989; Cleuren et al. 1995; McBrayer & White, 2002). To test skull performance under a variety of feeding behaviours we generated four primary static loading cases: distal/mesial and bilateral/unilateral bites. Mesial biting was simulated with an interdental beam between the 1st maxillary and 3rd dentary teeth and distal biting with an interdental beam between the 7th maxillary and 9th dentary teeth. These loading cases were solved for normal-bite (muscle induced tensional force only), pull-back (muscle induced tensional force plus 50 N force in longitudinal Z axis at the midpoint node of the interdental beam), and lateral-pull (muscle induced tensional force plus 50 N force in the transverse X-axis at midpoint node of the interdental beam). These give a total of 12 secondary loading cases. Eight of these cases, normal and pull-back in a distal/mesial bites, were tested for isotropic homogeneous (A–D groups are all of material 3) and heterogeneous material properties (A–D groups constituted of materials 1–4, respectively). This produced an overall total of 16 loading cases.

In our comparisons between models we focused on distributions of stress (internal force per unit area as a reaction of external loads applied), rather than strain (a quantification of deformation due to stress) largely because strain is more sensitive to alterations in the angle of force applied. Consequently, stress distributions will generally display closer agreement between isotropic and anisotropic models (Hylander, 1979; Dechow et al. 1993; Dechow & Hylander, 2000; Daniel & McHenry, 2001; Thomason et al. 2002; Rafferty et al. 2003; Metzger et al. 2005). For evaluating our results we concentrated on Von Mises (VM) stress, a good predictor of failure in ductile material such as bone (Rayfield, 2007) that can be used as a proxy for overall strength of the skull during each biting regime.

Results

In symmetrical mesial biting (normal), in which only the masticatory muscles are exerting a tensile load (Figs 2–4), relatively large VM stress areas are exhibited in the quadrate, squamosal and ventral cranium, as well as around the coronoid process, supra-angular, splenial, and lingual and occlusal dentary (Fig. 2). This stress distribution is observed in both heterogeneous and homogeneous models.

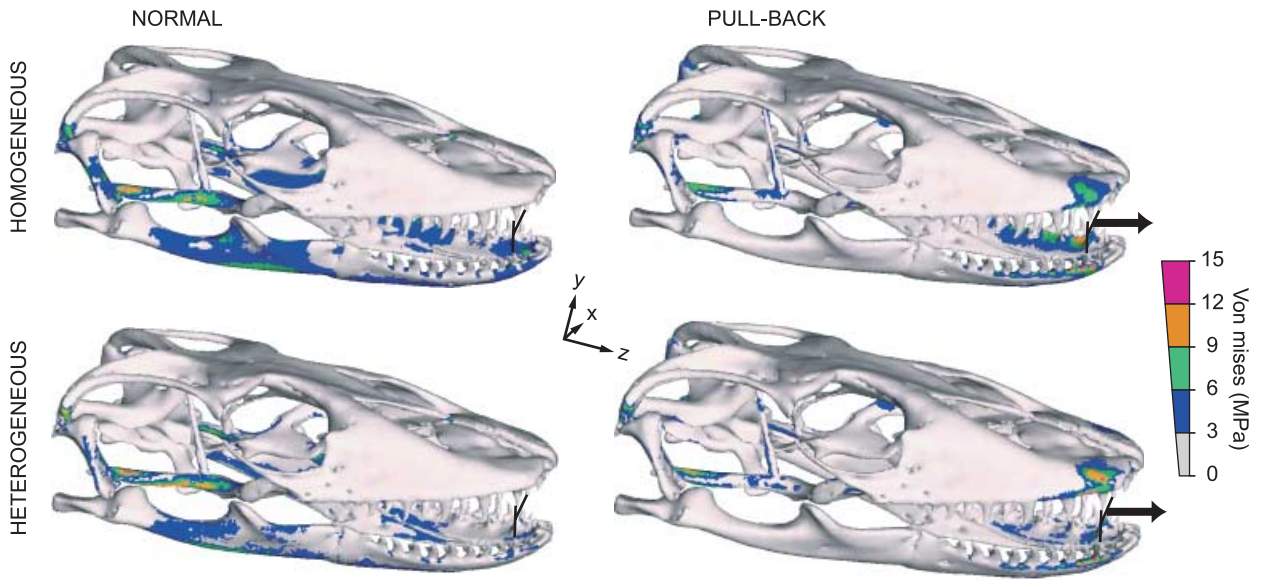

Fig. 2 Von Mises stress distribution for a symmetrical mesial bite in normal (action of masticatory muscles only) and pull-back load cases (i.e. combined actions of masticatory muscles plus additional loading that simulates a pull along the Z-axis by postcranial musculature): Muscle tensional force plus 50 N force (Z-axis), applied at the midpoint node of the interdental beam (arrow), for heterogeneous and homogeneous models. Peak stresses have been scaled out to minimize visual impact of model artefacts. Stress is more widely distributed in homogeneous than heterogeneous models but general patterns are preserved. In biting at a mesial point in the tooth row, stress is lower where an additional extrinsic load is applied (mesial pull-back bite) than where loading is restricted to masticatory muscles only (mesial normal bite).

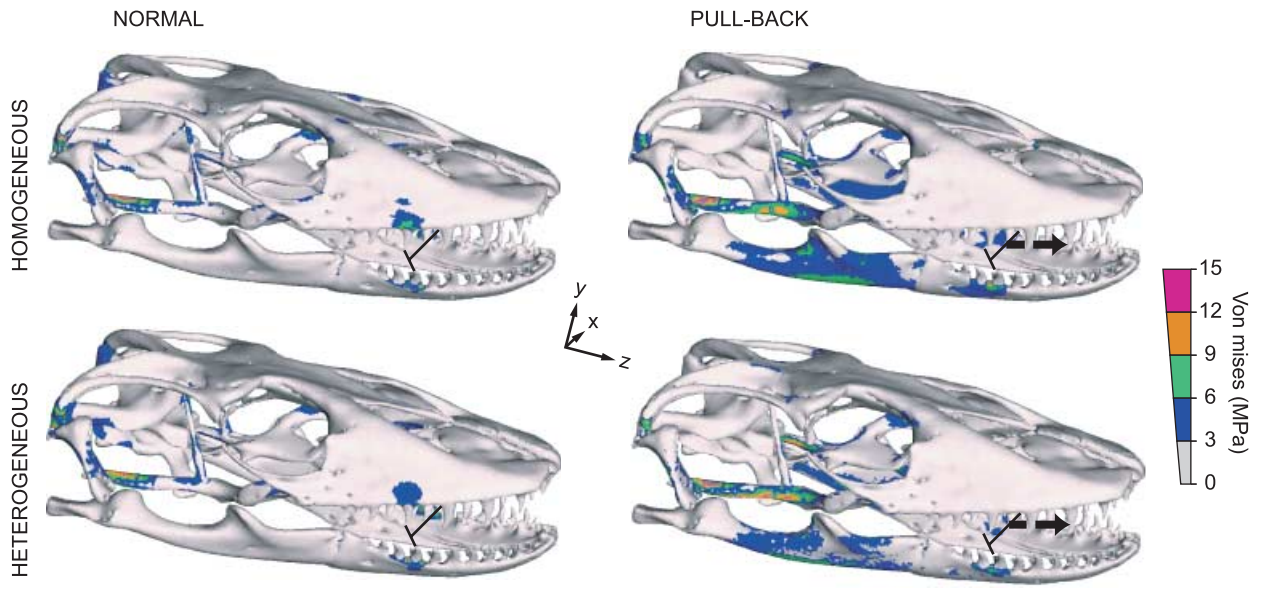

Fig. 3 Von Mises stress distribution in symmetrical distal bite in normal (action of masticatory muscles only) and pull-back load cases (i.e. action masticatory muscles plus additional loading that simulates a pull along the Z-axis by postcranial musculature): Muscle tensional force plus 50 N force (Z-axis) applied at the midpoint node of the interdental beam (arrow), for heterogeneous and homogeneous models. Peak stresses have been scaled out. In contrast to biting at an anterior point in the tooth row, when biting at a distal point, stress is lower when loading is restricted to masticatory muscles only (normal) and the addition of pull loading along the Z axis (pull-back) increases stress.

In symmetrical bites, the mesial pull-back (action of masticatory muscles plus 50 N force along the Z axis, which adds an extrinsic tensional force to the skull; Figs 2 and 4), high stress is located in the squamosal joint, quadrate, pterygoid, distal maxilla, premaxilla, and lingual dentary (Fig. 2). Similarly, a distal bite exhibits the greatest VM stress in the same regions as in the mesial pull-back bite, but in anterior regions of the skull, high stress is evident near the restraint area in the maxilla and dentary (Fig. 3). Conversely, the distal pull-back bite load case reveals high

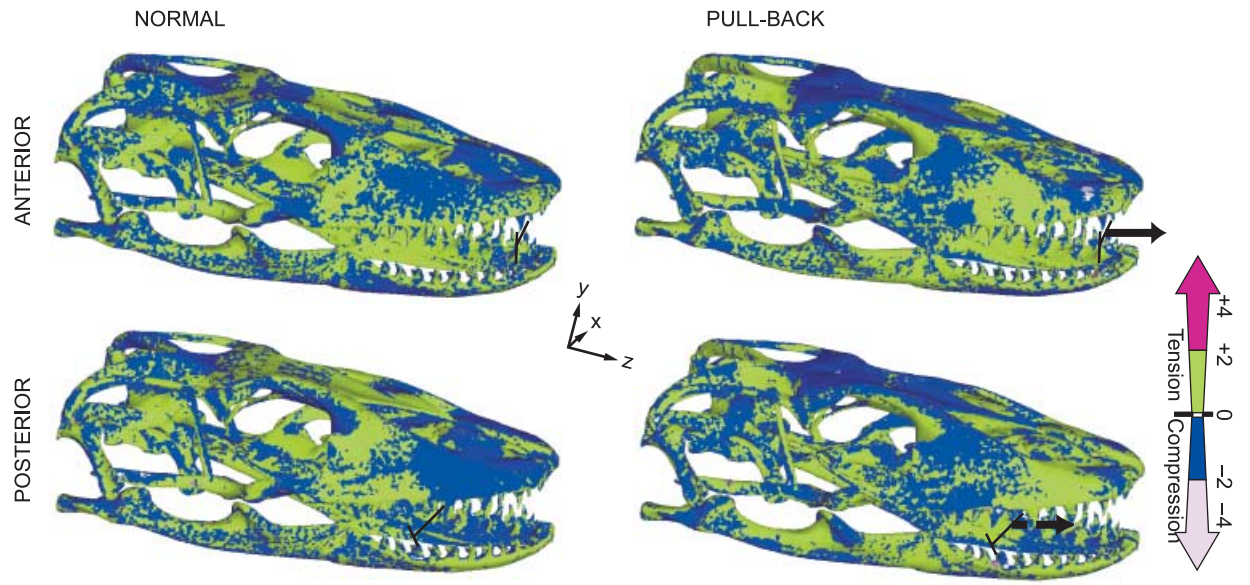

Fig. 4 Minimum principal stress distribution for heterogeneous models of symmetrical distal/mesial, normal/pull-back bite. Colour scale indicates compressive and tensile stress distributions. Peak stresses have been scaled out. Note that distal and mesial pull-back load cases receive higher compressive stress in the dorsal cranium, posterior maxilla, anterior quadrate and pterygoid-epipterygoid joint than in distal and mesial normal bites.

Table 2 Mean Von Mises 'brick' element stress in symmetrical load cases

Load cases	Heterogeneous (N)	Homogeneous (N)
Mesial normal bite	0.9067	1.0867
Distal normal bite	0.9108	1.0788
Mesial pull-back	0.6582	0.8459
Distal pull-back	0.8113	0.8593
Mesial lateral-pull	3.1449	–
Distal lateral-pull	2.6148	–

stress in the equivalent proximal skull zones seen in mesial-normal biting. Models showing the generally lowest VM stress are heterogeneous mesial pull-back and normal-distal bites (Figs 2 and 3).

In general, our heterogeneous models display more dispersed and lower mean VM stress under normal bite (~6%) and pull-back (16%) loads than in the respective homogeneous simulations (Table 2). When examined in more detail, resultant stress in the homogeneous models is more uniformly distributed throughout the whole structure (groups A–D), but in the heterogeneous model stress is re-distributed toward the stiffest materials (groups C and D), with the more elastic components displaying lower stress (groups A and B). Therefore, because heterogeneous models reveal high stresses in groups with comparatively much smaller volumes (C and D), overall VM stresses are greatly reduced in comparison with the homogeneous model, which places higher stresses in a representatively larger volume group (A and B; Table 1). Nonetheless, a general consistency between the stress patterns in both model types is observed in all loading cases. This is in broad agreement with results from Strait et al. (2005), obtained from comparisons of a modelled *Macaca* cranium in which selected regions were manually assigned different properties.

Heterogeneous normal bite load cases present high tensile stresses mainly in the occiput, prootic, proximal pterygoid and epipterygoid, nasal, and proximal maxilla regions; the proximal parietal is in compression (Fig. 4). In the mandible the tension/compression distribution is patchy, with tension in the proximal condyle, occlusal and proximal lingual regions and compression spread elsewhere. In contrast, pull-back load cases reveal high compressive stresses in the occiput, prootic, anterior pterygoid and epipterygoid, frontal and anterior parietal, and high tensile stresses in the proximal parietal and maxilla. However, similar tensile/compressive stress distribution is found in the mandible (Fig. 4). Homogeneous models display equivalent but broader dorsal compression and ventral tension in the cranium.

Results of mesial bite load cases differ from distal ones in the presence of tensile stress in the premaxilla and a compressed frontal in the mesial bite, which also shows distribution of compressive stress limited to the anterior lingual dentary. A distal bite generates tensile stress in the premaxilla and proximally extended compressive stress in the lingual dentary (Fig. 4). A distal-normal bite results in nearly equal overall VM stress in comparison with the mesial-bite.

Axial reaction force obtained at one of the interdental beams is ~4 N in mesial and ~9 N in distal biting (bite force for both jaws should be doubled). However, a mesial pull-back bite shows ~20% less VM stress than the distal one; and axial force at the interdental beams is ~8 N for mesial pull-back and ~10 N for distal pull-back (Fig. 3, Table 2).

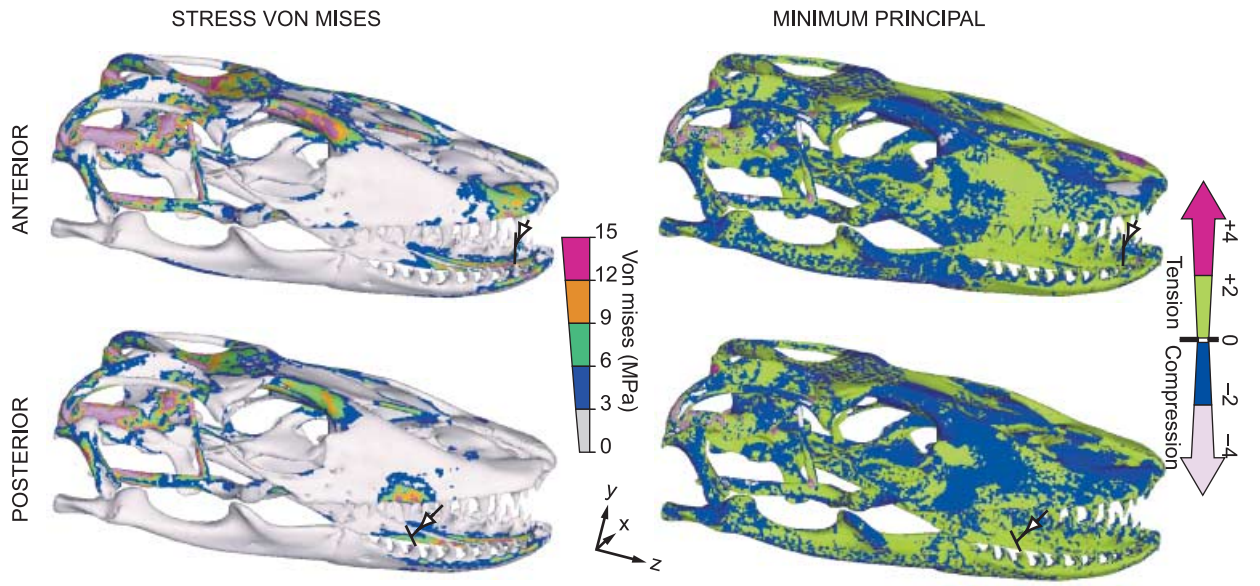

Fig. 5 Von Mises and minimum principal stress distributions for a symmetrical heterogeneous lateral-pull bite: Action of masticatory muscles plus lateral tensile force of 50 N (arrow) in distal/mesial load cases. Peak stresses have been scaled out. Note that high stress is scattered along the rostrum, contrasting with the low VM stress values observed in normal and pull-back load cases.

The symmetrical lateral-pull bite (Fig. 5), in which masticatory muscles are active and an additional lateral extrinsic force (50 N) is applied along the X-axis, shows the largest stress magnitudes of all the experiments. In this load case, simulating both jaw muscle-driven bite and postcranially generated lateral pull forces, the main areas with large VM stress in the biting side correspond to the squamosal [tension (t)], quadrate [compression (c)], prootic (t), pterygoid (mainly c), parietal (mainly t), prefrontal (c), nasopremaxilla (mainly c), and lingual dentary (t). High VM stress about the restraint areas is compressive in mesial and tensile in distal lateral-pull (Fig. 5). Stress distribution in the balancing side is characterized by high stress in these same areas, but a reversed distribution of tension/compression. Reaction forces obtained at one interdental beam in these simulations wherein prey is bitten and pulled laterally are ~18 N in mesial and ~15 N in distal bites (total bilateral forces would double these figures), indicating a moderately higher mechanical advantage at a mesial position relative to a distal one where an extrinsic force is also applied. This is consistent with greater torque due to a larger moment arm where an additional extrinsic load is applied anteriorly. However, a mesial lateral-pull bite presents up to 20% larger mean VM stress than a distal one.

Stress patterns for all asymmetrical (i.e. unilateral) bites generally follow those evident in symmetrical bites, although at the biting side this tends to increase proximally and decrease anteriorly by up to ~36% from the balancing one (Fig. 6). This pattern largely follows that described by Rafferty et al. (2003). However, the highly fenestrated cranial and non-tubular maxilla-palate morphology localizes stress, and does not present a continuous torsional loading.

In summary, our results show that:

1) Stress distribution in the proximal skull is similar in distal-normal and mesial pull-back simulations. These load cases produce the lowest overall stresses, particularly where heterogeneous material properties are incorporated. Conversely, mesial-normal and distal pull-back cases share general stress patterns and magnitudes that are higher than in equivalent asymmetrical load cases. However, stresses in mesial-normal and distal pull-back simulations are lower than in the symmetrical or asymmetrical lateral-pull cases. These similarities in stress distribution occur despite the differences in load and bite position (distal/mesial, normal/pull-back), which are largely limited to high stress areas near restraints (Figs 2 and 3).

2) Clear distinctions are apparent in tensile/compressive stress distribution between normal and pull-back load cases. During normal biting, high tensile stress is distributed in the occiput, prootic, nasal, and proximal maxilla but compressive stresses are concentrated in the posterior parietal and anterior maxilla regions. The reverse is true under pull-back loading (Fig. 4).

3) Distal and mesial biting load cases differ in the prevalence of either compressive or tensile stress in the premaxilla and a more posteriorly extended compressive stress in the lingual dentary in a distal load (Fig. 4). Overall, stress in a distal-normal bite is slightly higher than in a mesial one, while the opposite is true for pull-back load cases.

4) Differences between results obtained from heterogeneous and homogeneous models demonstrate a major role for bone elasticity in the reduction and allocation of stress, while not greatly impacting on broad VM or tensile/compressive patterns.

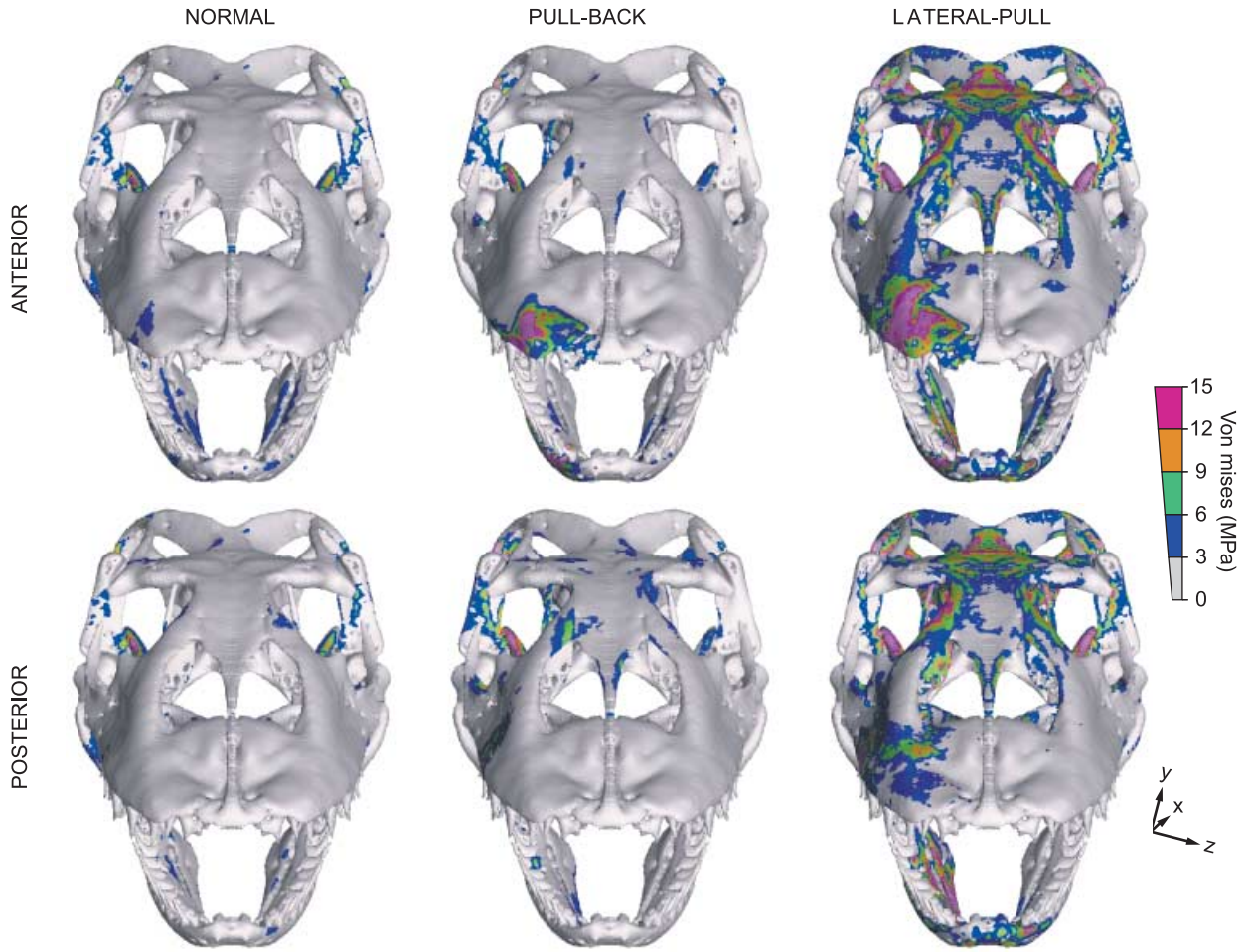

Fig. 6 Von Mises stress distribution for asymmetric (unilateral) bites in distal/mesial, and normal/pull-back/lateral-pull load cases. Peak stresses have been scaled out.

5) Symmetrical lateral-pull bites reveal larger stress in several skull zones with mixed tensile and compressive functions. These are most evident in the cranium, but are also found in the lingual dentary region. Areas near restraints show high compressive stress in medial, but tensile stress in distal, bites (Fig. 5).
6) A distal bite in normal and pull-back load cases presents higher bite force consistent with greater mechanical advantage. In contrast, during a lateral-pull, higher reaction forces are produced in the mesial tooth bite (Table 2).
7) Asymmetrical (unilateral) bites show higher stress overall in proximal balancing and mesial biting sides. This finding is in general agreement with results of Rafferty et al. (2003), but skull anatomy appears to localize stresses (Fig. 6).

Discussion

Implications of FE stress distributions for feeding ecology in the Komodo dragon

Given that, for two equivalently loaded structures, the one with lower and more dispersed stress will resist higher loads before catastrophic failure (Rayfield et al. 2001; Fastnacht et al. 2002; Rayfield, 2004, 2005; Preuschoft & Witzel, 2005; Moreno et al. 2007), we conclude that overall lower stresses exhibited in distal normal, lateral-pull, and mesial pull-back bites suggest that the skull of *V. komodoensis* is best adapted to perform these feeding behaviours.

These simulations demonstrate that overall skull stress magnitudes are mainly a consequence of mandibular load (Figs 2 and 3). During a distal bite the out-lever (muscle- to bite-position) is reduced. This also decreases mandibular torsion, because a restraint closer to the jaw joint will inhibit medial rotation caused by off-centre muscle tensile force (Smith, 1982). This bending reduction moderates general stress in normal and pull-back bites. However, the presence of an extrinsic 50 N lateral tensile force counteracts bending in the mesial lateral-pull model. This extrinsic force reduces medial torsion of the mandible and quadrate-articular joint compression because of reduction in mandible outward bending (wishboning). Stress distribution in the posterior cranium is focused in the quadrate, squamosal, and pterygoid in both normal and pull-back bites. Substantial

force is also received by the squamosal-quadrate joint. This may be a consequence of rigidity in the modelled quadrate-articular joint and limited *m. pterygoideus* quadrate-articular joint stabilization (see below). Consequently, our simulations of squamosal-quadrate deformation probably overestimate stress. However, despite the presence of these model artefacts, it is reasonable to suggest that the squamosal-quadrate joint will be under some flexion/extension loading due to the presence of streptostylic movement (Frazzetta, 1962, Metzger, 2002).

The pterygoid bone is stressed mainly in response to relatively large *m. pterygoideus* force production. However, we found different mechanical behaviour in the pterygoid depending on the presence/absence of longitudinal extrinsic loads. In normal bite simulations (absence of extrinsic loads), the epipterygoid-pterygoid joint is bent laterally via muscle tension action. In contrast, in pull-back simulations (presence of longitudinal extrinsic load) the epipterygoid-pterygoid joint is posteriorly flexed as the skull is pulled anteriorly and *m. pterygoideus* tension is counterbalanced.

Modelling limitations must be considered before further interpretation of these results. Our simulation of the *m. pterygoideus* comprises seven pretensioned trusses distributed in an equal number of muscle action lines (Fig. 1, Table 1). Although this architecture represents an improvement on the commonly used single point load (Strait et al. 2002; Dumont et al. 2005; Strait et al. 2006), it may still underestimate *m. pterygoideus* force and function. Our modelled *m. pterygoideus* does not simulate wrapping morphology nor does it fully replicate muscle pennation. Furthermore, in life the pterygoid is under more complex loads than any simulated here. *Protractor* and *levator pterygoideus* muscles, although proportionally much smaller (hence not included in the model), control some of the *m. pterygoideus* induced lateral bending and epipterygoid-pterygoid joint flexion generated by extrinsic longitudinal forces. These influences could reduce pterygoid stress. However, the *m. pterygoideus* also plays an important role restraining intra-mandibular joint flexion. This flexion function was not included in our modelled mandible, but in life it would transmit extra loads to the pterygoid complex. Consequently, the stress shown about the pterygoid, regardless of model limitations, is also likely to be high in real conditions.

High stress is located in the rostrum near the restraints in distal normal and mesial pull-back simulations, but is not observed in mesial normal and distal pull-back load cases. As explained above, this is mainly a consequence of the way in which the mandible is loaded, which not only results in lower overall stress, but also application of a greater bite force. Note that mesial normal loading produces almost 45% less bite force, but reveals similar stress magnitudes to the distal normal loading. Hence, a mesial normal bite is weak relative to a distal normal bite.

Regarding pull-back load cases, of particular interest is our observation that although mesial pull-back loading generates 20% less force, in this case the skull is under 20% less stress than during distal pull-back loading. Therefore, considering these proportions and the linearity of the model, a distal pull-back would apply equivalent bite force to that of a mesial pull-back load without increasing skull stress. This key feature of performance in the skull of *V. komodoensis* strongly suggests that the structure is far better optimized to simultaneously apply a jaw adductor-driven bite and postcranially generated pull-back, as opposed to a solely jaw driven (normal) bite.

This conclusion is further supported by clear evidence for multiple adaptations facilitating the rearward distribution of the loads in both symmetric and asymmetric bites. These include the triangular shape of the maxilla and its proximal and elongated contact surface with the frontal, which distribute the compressive force generated when biting toward the frontal and parietal; light anterior skull construction in comparison with the posterior one; and forward direction of the splenial-dentary suture, which easily transmit loads to the rest of the mandible. Additionally, the *m. adductor mandibulae* and *m. pseudotemporalis* contribute to mandibular retraction/protraction, due to largely dorsoposteriorly/ventroanteriorly orientation of muscle fibres. Only a small portion of the *m. adductor mandibulae* is dorsoventrally oriented (MAEMa). Together with the *m. pseudotemporalis profundus*, also a minor muscle, these are the main mandibular elevators.

During a lateral-pull, high stress is distributed in the prootic, parietal, prefrontal and nasal bones as well as in the squamosal, quadrate and pterygoid. This is likely because the lateral extrinsic force applied on the maxilla produces a compressive force against the prefrontal, septomaxilla and nasal in the biting side. Moreover, consequent lateral bending of the mandible generates a large lateral bending in the squamosal-quadrate joint, which is extended toward the prootic. Model artefacts discussed above may have amplified this effect. Also, lateral bending of the mandible produces posterior flexion of the epipterygoid-pterygoid joint, protracting the rostrum.

Our modelling suggests that the *V. komodoensis* skull is poorly adapted to resist a lateral-pull bite. Although the heterogeneous model accounts for differences in material properties within the bone, it does not include connective tissue, which in life might further reduce overall stress (and see below). Uncertainty exists regarding just how much reduction this would imply. However, comparisons made between distal and mesial bites within the same model, indicate that a mesial lateral-pull bite generates 20% larger force, whereas a distal one produces 20% less overall stress. This means that distal and mesial bites are proportionally equivalent under linear conditions and that the Komodo dragon could be equally adapted for a lateral-pull at any bite point. Our modelling further

suggests that the skull can withstand large asymmetrical loads without compromising the overall structure.

Additional differences in bone performance were observed between heterogeneous and homogeneous models. Homogeneous modelling reveals equivalent heterogeneous high stress zones, but also produces expanded stress areas. These zones amplify overall stress. The only cases in which this difference diminishes are in mesial pulling bites (lateral as well as pull-back). These results relate directly to the lower stiffness and thin contact of the premaxilla-maxilla suture. This is best exemplified in stress distribution under distal pull-back loading, which shows more proximally extended tensile stress in the anterior maxilla and greater compression in the premaxilla in the heterogeneous relative to the homogeneous model (Fig. 3). A real skull might present even more marked tensile/compressive patterns because of variation in material properties of the bone and other connective tissues. We may also expect to see a degree of functional compartmentalization in different skull regions and structures, and consequent 'insulation' against high loads (Rafferty & Herring, 1999; Herring & Teng, 2000; Rafferty et al. 2003).

Our data are consistent with the animal's documented defleshing techniques, particularly with respect to the relative motion of the rostrum. When processing a carcass, *V. komodoensis* rotates the muzzle in both the lateral and posterior directions simultaneously (Auffenberg, 1981). This results in varied direction and intensity of forces along the muzzle.

In addition to securing the prey item, the distal teeth are the first to enter the substrate and are closest to the occiput. These teeth are drawn mostly in the posterior direction with relatively little lateral movement, but larger bite force. Conversely, the mesial teeth are further away from the occiput and are laterally and posteriorly driven by a combination of rotational neck movements and full body longitudinal tensile force (pull-back). Our data indicates that the occiput is better suited to withstand forces in the direction of pull-back loading, whereas anteriorly, the skull performs better for a lateral-pull with a far more evenly distributed load along the rostrum.

We conclude that in large part our FE model of the Komodo dragon skull faithfully reproduces qualitative observational data on feeding behaviour of the animal. This in turn suggests that similar techniques can be applied to assist in the prediction of behaviour for taxa of unknown habits, both living and extinct. Models such as those generated in the present study may be useful in the study of a range of further questions, such as the role of cranial kinesis in varanids and other reptiles (work in progress).

Comparison with other extant and extinct taxa

Our estimates of muscle force generated by *V. komodoensis* mandible adductors were surprisingly low (90 N each side, Table 1) for a 1.6-m-long lizard. The alignment of muscle fibres, mostly at an acute angle to the mandible, together with the low modelled gape (15º), are likely to have further contributed to weak bite reaction forces. Maximum bite force obtained was around 10–20 N. However, if the same model had a larger gape, the muscle would have gained extra mechanical advantage and larger moments in the jaw articulation would have produced stronger bites. The animal might also have been capable of generating large angular accelerations to the jaw at the beginning of a snapping bite (Sinclair & Alexander, 1987). Other factors acting to reduce bite reaction forces in the model include the slightly protracted quadrate orientation and elastic deformation of interdental beams. Moreover, the storage of strain energy in more elastic regions of our heterogeneous model is likely to have resulted in a reduction of force available at bite points (Wroe et al. 2007b). However, although consideration of these complicating factors suggests that bite reaction forces taken from our model may be sub-maximal, results of estimates using 2D techniques together with *in vivo* data from captive *V. komodoensis* strongly imply that our 3D-based predictions do not greatly underestimate bite force.

Using 2D methodology to predict bite forces in a much smaller varanid (*V. bengalensis* – 2.6 kg body mass, 5 cm head length), Sinclair & Alexander (1987), obtained forces of 5 N–13 N in vertical mesial and distal bite positions respectively. Applying this 2D calculation to our much larger *V. komodoensis* specimen gives bite reaction forces of 11 N and 16 N at the same bite points. The weak bite of the Komodo dragon may be in part explained by the fact that its condyle is positioned more anteriorly than that of *Varanus bengalensis*, conferring relative mechanical advantage to the latter.

Herrel et al. (1999a) measured ~2.38–109 N *in vivo* bite force for specimens of the lizard *Gallotia galloti* ranging from 1.5 to 3 cm in head length. The skull of this species is around 23–26% of the snout-vent length (SVL), while the head length of the *V. komodoensis* we studied is only 15% of SVL. In comparing estimated bite forces between different species, including small crocodiles and turtles, Sinclair & Alexander (1987) concluded that varanids in general produced comparatively small bite forces among Reptilia.

Thus, overall, our results are consistent with previous findings that varanids produce relatively weak bite reaction forces, and further, that bite force in the Komodo dragon is weak among varanids.

With respect to pulling forces, gauge data obtained from two captive *V. komodoensis* (specimens 98R046 and 98R069, Miami Metro Zoo) with similar head length (~16 cm) to the one modelled in the present study (14 cm), indicate that they are capable of exerting forces exceeding the equivalent of half their body mass (~170 N). These specimens were fed regularly, and appeared to be relatively sated. Increased hunger might reasonably result in higher

level of 'enthusiasm' and higher pull forces. These results suggest that postcranial musculature in the Komodo dragon is capable of delivering forces that may exceed those of the jaw elevators by an order of magnitude or more.

Nonetheless, jaw adductor-driven bite force is a factor to be considered in the understanding of predatory behaviour in any carnivorous vertebrate. A well-demonstrated relationship between bite force and feeding ecology has been established among extant mammalian carnivores (Wroe et al. 2005; Christiansen & Wroe, 2007). These authors observe that this cannot be considered a universal relationship where taxa under consideration exhibit unique adaptations, even within Mammalia. Wroe et al. (2005) predicted relatively low bite force in the highly specialized fossil sabrecat *Smilodon fatalis*, but concluded that this indicated unique killing behaviour, wherein a combination of extraordinary tooth morphology and the recruitment of cervical musculature facilitated predation tactics unknown among living cats. Extant felids typically deploy a crushing bite to the posterior cranium or cervical vertebra in small- to medium-sized prey, or a prolonged suffocating bite to the neck of large prey. In contrast, it is likely that *S. fatalis* rarely took small-medium prey and applied a 'canine-shear bite' to soft tissues of large prey that produced major trauma and a quick kill (McHenry et al. 2007), an obvious advantage being minimization of physical threat to the predator. Broad analogy has been made between this approach and that of *V. komodoensis* (Akersten, 1985).

Varanus komodoensis shares anatomical features with some theropod dinosaurs, such as *Allosaurus* and the abelisaurid *Majungasaurus.* All have serrated blade-like teeth, gracile well-fenestrated skulls, and long rostra. A notable difference is that relative to *V. komodoensis*, these dinosaurs have laterally compressed crania (taller than wide), and consequently might be expected better to resist dorsoventral loads. We also predict that differences between working and balancing sides will be less marked than is evident in the dorsoventrally compressed cranium of the Komodo dragon. On the other hand, reconstruction of tyrannosaurid neck musculature by Snively & Russell (2007) suggests that tyrannosaurids, with broad dental arcades and high leverage for lateroflexive neck muscles, could have engaged in a similar defleshing technique to that of *V. komodoensis*. In some ways these tyrannosaurids, as well as extant crocodilians, may represent a closer comparison to the Komodo dragon than other tall-skulled carnivorous archosaurs. However, their more robust cranial and dental morphology also suggests different mechanical and feeding behaviour in other respects (Rayfield, 2004, 2007; Barrett & Rayfield, 2006; McHenry et al. 2006; Snively et al. 2006) that probably involved more puncture-and-tear excision of flesh than the efficient slicing evident in the Komodo dragon.

Conclusions

We demonstrate correspondence between our observed and previously published Komodo dragon feeding behaviour (Auffenberg, 1981), morphological adaptations in its feeding apparatus, bite reaction forces and mechanical behaviour as revealed by our 3D FE modelling. We conclude that the skull and associated musculature of *V. komodoensis* are particularly well-adapted to exert and resist forces generated during pull-back biting. The posterior rostrum presents extra mechanical advantage to hold the prey and withstand pull-back loads imposed by retraction of its skull, and the anterior part is equally well adapted for exerting lateral pull bites.

The highly fenestrated, lightweight skull of *V. komodoensis* is optimized to resist a complex and finely balanced combination of adductor forces and loads generated by cervical and other postcranial muscles during killing and feeding. This combination of anatomical and behavioural features, together with its markedly ziphodont dentition, allows the animal to kill and deflesh large prey efficiently, using relatively low jaw adductor driven bite force.

Further studies will better distinguish differences between stress distributions under different loading conditions and lead to improved model characteristics and validation.

Acknowledgements

Thanks to Ross Sadler (Australian Museum), Patrick Cooper and Scott Hocknull (Queensland Museum) for access to the specimen. Funded by ARC Discovery, ARC QE2 Research Fellowship and UNSW Strategic Research Initiatives grants to S. Wroe, and an Internal Grant (Univ. of Newcastle) to P. Clausen.

References

Akersten WA (1985) Canine function in *Smilodon* (mammalia; felidae; machairodontinae). *Contrib Sci* **356**, 1–22.

Auffenberg W (1981) *The Behavioral Ecology of the Komodo Monitor*. Gainesville: University Presses of Florida.

Barrett PM, Rayfield EJ (2006) Ecological and evolutionary implications of dinosaur feeding behaviour. *Trends Ecol Evol* **21**, 217–224.

Busbey ABI (1989) Form and function of the feeding apparatus of *Alligator mississippiensis*. *J Morphol* **202**, 99–127.

Christiansen P, Wroe S (2007) Bite forces and evolutionary adaptations to feeding ecology in carnivores. *Ecology* **88**, 347–358.

Cleuren J, Aerts P, De Vree F (1995) Bite and joint force analysis on *Caiman crocodilus*. *Belg J Zool* **125**, 79–94.

Daniel WJT, McHenry CR (2001) Bite force to skull stress correlation: modelling the skull of *Alligator mississippiensis*. In *Crocodilian Biology and Evolution* (eds Seebacher F, Franklin CE), pp. 135–143. New South Wales, Australia: Surrey Beatty & Sons.

Dechow PC, Hylander WL (2000) Elastic properties and masticatory bone stress in the macaque mandible. *Am J Phys Anthropol* **112**, 553–574.

Dechow PC, Nail GA, Schwartz-Dabney CL, Ashman RB (1993) Elastic properties of human supraorbital and mandibular bone. *Am J Phys Anthropol* **90**, 291–306.

Dumont ER, Piccirillo J, Grosse IR (2005) Finite-element analysis of biting behavior and bone stress in the facial skeletons of bats. *Anat Rec Part A* **283**, 319–330.

Elias JA, McBrayer LD, Reilly SR (2000) Prey transport kinematics in *Tupinambis teguixin* and *Varanus exanthematicus*: conservation of feeding behavior in 'chemosensory-tongued' lizards. *J Exp Biol* **203**, 791–801.

Fastnacht M, Hess N, Frey E, Weiser H-P (2002) Finite element analysis in vertebrate paleontology. *Seckenbergiana Lethaea* **82**, 195–206.

Frazzetta T (1962) A functional consideration of cranial kinesis in lizards. *J Morphol* **111**, 287–320.

Haas G (1973) Muscles of the jaws and associated structures in the rhyncocephalia and squamata. In *Biology of the Reptilia* (eds Gans C, Parsons TS), pp. 285–490. London and New York: Academic Press.

Herrel A, Aerts P, De Vree F (1998) Static biting in lizards: functional morphology of the temporal ligaments. *J Zool* **244**, 135–143.

Herrel A, Spithoven R, Van Damme R, De Vree F (1999a) Sexual dimorphism of head size in *Gallotia galloti*: testing for niche divergence hypothesis by functional analysis. *Funct Ecol* **13**, 289–297.

Herrel A, Verstappen M, De Vree F (1999b) Modulatory complexity of the feeding repertoire in scincid lizards. *J Comp Physiol A* **184**, 501–518.

Herring SW, Teng S (2000) Strain in the braincase and its sutures during function. *Am J Phys Anthropol* **112**, 575–593.

Hylander WL (1979) Mandibular function in *Galago crassicaudatus* and *Macaca fascicularis*: an in vivo approach to stress analysis in the mandible. *J Morphol* **159**, 253–296.

Mayes PJ, Thompson GG, Withers PC (2005) Diet and foraging behaviour of the semi-aquatic *Varanus mertensi* (Reptilia: Varanidae). *Wildlife Res* **32**, 67–74.

McBrayer LD, White TD (2002) Bite force, behavior, and electromyography in the teiid lizard tupinambis teguixin. *Copeia* **2002**, 111–119.

McHenry CR, Clausen PD, Daniel WJT, Meers MB, Pendharkar A (2006) Biomechanics of the rostrum in crocodilians: a comparative analysis using finite-element modeling. *Anat Rec Part A* **288**, 827–849.

McHenry CR, Wroe S, Clausen PD, Moreno K, Cunningham E (2007) Super-modeled sabercat, predatory behaviour in Smilodon fatalis revealed by high-resolution 3-D computer simulation. *Proc Natl Acad Sci USA* **104**, 16010–16015.

Mertens R (1942) Die Familie der warane (Varanidae). *Abh Senckenbergische Naturforsch Ges* **465**, 1–39.

Metzger K (2002) *Cranial Kinesis in Lepidosaurus: Skulls in Motion*. New York: Shaper Publishing.

Metzger KA, Daniel WJT, Ross CF (2005) Comparison of beam theory and finite-element analysis with in vivo bone strain data from the alligator cranium. *Anat Rec Part A* **283**, 331–348.

Moreno K, Carrano MT, Snyder R (2007) Morphological changes in pedal phalanges through ornithopod dinosaur evolution: a biomechanical approach. *J Morphol* **268**, 50–63.

Preuschoft H, Witzel U (2005) Functional shape of the skull in vertebrates: which forces determine skull morphology in lower primates and ancestral synapsids? *Anat Rec Part A* **283**, 402–413.

Rafferty KL, Herring SW (1999) Craniofacial sutures: morphology, growth, and in vivo masticatory strains. *J Morphol* **242**, 167–179.

Rafferty KL, Herring SW, Marshall CD (2003) Biomechanics of the rostrum and the role of facial sutures. *J Morphol* **257**, 33–44.

Rayfield EJ (2004) Cranial mechanics and feeding in *Tyrannosaurus rex*. *Proc R Soc London B Biol Sci* **271**, 1451–1459.

Rayfield EJ (2005) Aspects of comparative cranial mechanics in the theropod dinosaurs Coelophysis, Allosaurus and Tyrannosaurus. *Zool J Linn Soc* **144**, 309–316.

Rayfield EJ (2007) Finite element analysis and understanding the biomechanics and evolution of living and fossil organisms. *Annu Rev Earth Planet Sci* **35**, 541–576.

Rayfield EJ, Norman DB, Horner CC, et al. (2001) Cranial design and function in a large theropod dinosaur. *Nature* **409**, 1033–1037.

Reilly SM, McBrayer LD, White TD (2001) Prey processing in amniotes: biomechanical and behavioural patterns of food reduction. *Comp Biochem Physiol* **128A**, 397–415.

Rho JY, Hobarto MC, Ashman RB (1995) Relations of mechanical properties to density and CT numbers in human bone. *Med Eng Phys* **17**, 347–355.

Schneider U, Pedroni E, Lomax A (1996) The calibration of CT Hounsfield units for radiotherapy treatment planning. *Phys Med Biol* **41**, 111–124.

Sinclair AG, Alexander RM (1987) Estimates of forces exerted by the jaw muscles of some reptiles. *J Zool* **213**, 107–115.

Smith KK (1982) An electromyographic study of the function of the jaw adducting muscles in *Varanus exanthematicus* (Varanidae). *J Morphol* **173**, 137–158.

Snively E, Russell AP (2007) Functional variation of neck muscles and their relation to feeding style in tyrannosauridae and other large theropod dinosaurs. *Anat Rec* **290**, 934–957.

Snively E, Henderson DM, Phillips DS (2006) Fused and vaulted nasals of tyrannosaurid dinosaurs: implications for cranial strength and feeding mechanics. *Acta Palaeontol Pol* **51**, 435–454.

Strait D, Richmond B, Ross C, Spencer M (2002) Finite element analysis of a macaque skull: applications for functional morphology. *Am J Phys Anthropol* **177**, Suppl. 34, 149.

Strait DS, Wang Q, Dechow PC, et al. (2005) Modeling elastic properties in finite element analysis: how much precision is needed to produce an accurate model? *Anat Rec Part A* **283**, 275–287.

Strait DS, Wright BW, Richmond BG, et al. (2006) Craniofacial strain patterns during premolar loading: implications for australopithecus feeding. *Am J Phys Anthropol* **129**, 173.

Thomason JJ (1995) *Functional Morphology in Vertebrate Paleontology*. Cambridge: Cambridge University Press.

Thomason JJ, McClinchey HL, Jofriet JC (2002) Analysis of strain and stress in the equine hoof capsule using finite element methods: comparison with principal strains recorded in vivo. *Equine Vet J* **34**, 719–725.

Watts PC, Buley KR, Sanderson S, Boardman W, Ciofi C, Gibson R (2006) Parthenogenesis in Komodo dragons. *Nature* **444**, 1021.

Wroe S, McHenry CR, Thomason JJ (2005) Bite club: comparative bite force in big biting mammals and the prediction of predatory behaviour in fossil taxa. *Proc R Soc Lond B Biol Sci* **272**, 619–625.

Wroe S, Clausen PD, McHenry CR, Moreno K, Cunningham E (2007a) Computer simulation of feeding behaviour in the thylacine and dingo: a novel test for convergence and niche overlap. *Proc R Soc London B Biol Sci* **274**, 2819–2828.

Wroe S, Moreno K, Clausen PD, McHenry CR (2007b) High-resolution computer simulation of hominid cranial mechanics. *Anat Rec* **290**, 1248–1255.